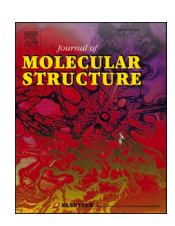
ELSEVIER

Contents lists available at ScienceDirect

# Journal of Molecular Structure

journal homepage: www.elsevier.com/locate/molstr





# Crystal structure, supramolecular features and antibacterial activities of a Cu(II) Schiff base complex using a bidentate $N_2O_2$ donor Schiff base ligand

Udaya Kumar AH <sup>a,f</sup>, Mahesha <sup>a,b</sup>, Jyothi KL <sup>c</sup>, Akil Ahmad <sup>d</sup>, Mohammed B Alshammari <sup>d</sup>, Karthik Kumara <sup>e</sup>, Lokanath NK <sup>a,\*</sup>

- <sup>a</sup> Department of Studies in Physics, University of Mysore, Manasagangotri, Mysuru 570 006, Karnataka, India
- <sup>b</sup> Department of Physics, SJCE, JSS Science and Technology University, Mysuru 570 006, Karnataka, India
- <sup>c</sup> Department of PG Physics, Government First Grade College and PG Center, Chintamani 563 125, India
- d Department of Chemistry, College of Sciences and Humanities, Prince Sattam bin Abdulaziz, University Al-Kharj 11892, Saudi Arabia
- <sup>e</sup> Department of Physics B.M.S. College of Engineering Bengaluru 560 019, Karnataka, India
- f Department of Physics, Seshadripuram Institue of Technology, Kadakola Industrial Area, Mysuru-571311, Karnataka, India

#### ARTICLE INFO

Original content: CCDC No. 2352425 (Original data)

Keywords: Schiff base Copper complex Crystal structure Computational studies Antibacterial studies

#### ABSTRACT

Bi-dentate N, O mononuclear Cu(II) complex  $[Cu(C_{14}H_{12}BrNOS)_2]$  was synthesized and characterized by FTIR spectroscopy. Single-crystal X-ray diffraction studies reveal the Cu(II) complex crystallizes in a monoclinic  $P2_1/c$  space group. The mononuclear copper complex comprises four coordinates with perfect square planar geometry ( $\tau_4$ =0). The copper complex shows C—H···Br and C—H···C interaction, respectively, enables the formation of multi-dimensional supramolecular architecture. The nature of the above intermolecular interactions is quantified by Hirshfeld surface analysis. The strength of the interaction and 3D topology of crystal packing are visualized through an energy framework.

Further, the physical nature of intramolecular interactions is assessed by QTAIM, the NCI index model. The theoretical approach based on DFT was employed to evaluate the optimized electronic structure, HOMO-LUMO, energy gap, molecular properties and global parameters. The copper complex exhibits good antibacterial activity against *S. aureus*. The molecular docking of the copper complex shows good binding affinity towards *S. aureus TyrRS*.

## 1. Introduction

Schiff bases exhibit structural diversity due to the wide range of primary amines and carbonyl compounds available for their synthesis. This structural variability contributes to the versatility of Schiff bases and their metal complexes in coordination chemistry [1]. They are indeed fascinating ligands due to their easy tunability of stereo-electronic structures, which allows for precise control over their molecular structure and functional groups. As a result, Schiff bases can be tailored to match the coordination preferences of transition metals, leading to the formation of stable complexes [2]. Further, the stable complexes formed between Schiff bases and transition metals exhibit diverse structural, electronic, and reactivity properties, which can be further modulated by modifying the Schiff base structure [3–6]. This versatility makes Schiff bases indispensable in the design and synthesis of functional coordination complexes for applications in drug design,

catalysis, materials science, medicinal chemistry, and other fields [7-11].

The recent upsurge of activities in the field of metal-based compounds, including nonclassical platinum complexes, reflects a growing interest in developing novel therapeutic agents with distinct mechanisms of action compared to traditional drugs like cisplatin [12]. This surge is driven by the need to overcome limitations such as resistance and toxicity associated with existing chemotherapy agents. Researchers are focusing on leveraging structural information to design and synthesize metal-based compounds with enhanced safety profiles and improved cytotoxicity [9,13]. This involves modifying existing chemical structures through ligand substitution or creating entirely new compounds with optimized properties and an enhanced cytotoxic and pharmacokinetic profile. Overall, the exploration of metal-based compounds represents a promising avenue for the development of novel antibacterial agents [14–16].

E-mail address: lokanath@physics.uni-mysore.ac.in (L. NK).

<sup>\*</sup> Corresponding author.

In this study, we have synthesized and spectroscopically characterized the new copper (II) Schiff-base complex and elucidated their structural features using single-crystal X-ray diffraction. We have employed a DFT approach to calculate various quantum chemical parameters of these complexes, which allows us to understand the electronic structure, stability, and reactivity of the complexes. It is relevant in estimating chemical reactivity concepts of bioactive metal complexes, as they provide valuable insights into electron distribution and compound reactivities. Overall, this comprehensive approach combining experimental characterization techniques with computational modelling allows us to gain a deeper understanding of the structural, electronic, and pharmacological properties of the synthesized copper(II) Schiff-base complexes. This knowledge contributes to the exploration of their potential applications as drug candidates in various therapeutic areas.

#### 2. Methods and materials

All chemicals used for the experiment were of analytical grade and were purchased from TCI India and Sigma-Aldrich. They were utilized without the need for additional purification. The Fourier transform infrared (FT-IR) spectra were recorded within the range of 500–4000 cm<sup>-1</sup> using *PerkinElmer* Spectrum Version 10.03.09 and depicted in Figure S1. The SEM and EDAX analyses were carried out using the *ZEISS EVO* instrument (Figure S2).

#### 2.1. Synthesis of copper complex

2-(methylthio)aniline (1 mmol, 0.139 g) was dissolved in 10 mL of methanol and added to a 10 mL methanolic solution of 5-bromosalicylal-dehyde (1 mmol, 0.201 g). The resulting yellow reaction mixture was heated to 60  $^{\circ}\text{C}$  and refluxed for 2 h. After cooling, the solution was filtered to remove the yellow-colored precipitate, which was then dried in a vacuum chamber.

Subsequently, copper acetate monohydrate (1 mmol, 0.199 g) in 20

mL of methanol solvent was added to a 10 mL methanolic solution of the Schiff base ligand (1 mmol 0.322 g) with constant stirring at 60 °C for 6 h. A red-coloured precipitate formed, which was filtered out. The resulting methanolic solution of the copper complex was subjected to slow evaporation. Good quality orange-coloured crystals were obtained from the filtrate after 20 days. A schematic representation of copper synthesis is shown in Scheme 1. Yield: 48 %. The melting point is found to be 230 °C. FT-IR (KBr),  $\nu$  cm<sup>-1</sup>: 1605.00 cm<sup>-1</sup> (C=N), 1162.77 cm<sup>-1</sup> (C-O Phenolic), 3051.00 cm<sup>-1</sup> (C-H, aromatic) and 751.1 cm<sup>-1</sup> (C-Br).

## 2.2. Single crystal X-ray diffraction (SXRD)

Single crystal X-ray diffraction is the only non-destructive analytical technique which provides complete 3D structural information of the crystalline sample. X-ray intensity data was collected on a Rigaku Xtalab mini single crystal X-ray diffractometer using graphite monochromator and MoK<sub> $\alpha$ </sub> radiation ( $\lambda = 0.71073$  Å, 293 K). The complete data were processed using the d\*trek program, and absorption correction was conducted with the multi-scan employed in the CrystalClear progra [17]. The crystal structures of the complexes were solved by direct methods (SHELXT), and the position of all non-hydrogen atoms was identified and refined on  $F^2$  by a full-matrix least-squares procedure using anisotropic displacement parameters (SHELXL) [18,19]. All the hydrogen atoms were located in difference Fourier maps and treated as riding on their parent atoms with isotropic thermal displacement parameters [Uiso(H) = 1.2Ueq(CH, CH<sub>2</sub>) and Uiso(H) = 1.5Ueq(CH<sub>3</sub>)]. The geometrical calculations and crystal packing diagrams were prepared by the crystallographic program PLATON [20] and MERCURY 4.2.0 [21] software.

#### 2.3. Hirshfeld surface analysis

Hirshfeld surface analysis (HSA), which is carried out using the *CrystalExplorer* 17.5 software is one of the best methods for the Investigation of intermolecular interactions in the crystalline environment

Scheme 1. Synthesis pathway of Schiff base ligand and its copper complex.

[22,23]. The HS enclosing a molecule is defined by points where the contribution to the electron density from the molecule of interest is equal to the contribution from all the other molecules. The molecular Hirshfeld surface mapped with 3D  $d_{\rm norm}$  was produced using  $d_{\rm e}$  and  $d_{\rm i}$  values, and the van der Waal's atomic radii (r) were governed by the Eq. (1) given below.

$$d_{norm} = \frac{d_i - r_i^{\nu dw}}{r_i^{\nu dw}} + \frac{d_e - r_e^{\nu dw}}{r_e^{\nu dw}}$$

$$(1)$$

Here  $d_i$  is the distance from a given point on the Hirshfeld surface to the nearest nucleus inside the surface, and  $d_e$  is the distance from a point to the nearest nucleus outside the surface.

The coloured regions (Red-White-Blue) on the  $d_{norm}$  surface represent different intermolecular interactions. The red color on the HS represents –ve values of  $d_{\text{norm}}$ , which gives the locations of short contacts shorter than the sum of van der Waals radii, the white color represents zero value of  $d_{\text{norm}}$ , which indicates those contacts for which intermolecular distances are almost equal to van der Waals radii, whereas blue color represents +ve values of  $d_{norm}$  which shows those contacts for which intermolecular distances are longer than the sum of van der Waals radii. This software can also be used to generate other surfaces:  $d_i$ (distance from HS to the nearest atom internal (i) to the surface),  $d_{\rm e}$ (distance from HS to the nearest atom external (e) to the surface), shape index (function depends on the HS flatness or curvature), curvedness (function depends on the HS concavity or convexity) and fragment patch (unique (coloured) region based on atoms external to the HS designed to indicate the nearest-neighbouring molecule). These surfaces will provide direct insight into the intermolecular  $\pi$ -  $\pi$  stacking interactions. Further, globularity (G), which is defined as the ratio of a sphere's surface area to HS's surface area, having the same volume as a sphere. The asphericity  $(\Omega)$  which is a measure of anisotropy of the molecule, was also found out from the HSA [22,24,25].

#### 2.4. Energy frameworks analysis

One can generate two-dimensional fingerprint plots (2D FPs) for three-dimensional HS by using the same software by considering  $d_{\rm i}$  and  $d_{\rm e}$  distances as a pair of coordinates, in intervals of 0.01 Å, for each individual spot on the HS. The contacts between selected atoms inside the HS and the atoms outside of it, including reciprocal contacts have been generated in percentage contribution. These FPs can be generated for all possible contacts between the elements by which the molecule is made off and measurements bond lengths, bond angles and torsion angles can also be measured.

Further, pairwise intermolecular interaction energies in the crystalline environment were calculated from the monomer wave functions using CE-HF/6-31G energy model. The molecular interaction energies such as electrostatic, polarization, dispersive and repulsive energy were also computed which leads to the total interaction energy as given by

$$E_{tot} = E_{ele} + E_{pol} + E_{dis} + E_{rep}$$

$$E_{tot} = k_{ele} E_{ele}^{\prime} + k_{pol} E_{pol}^{\prime} + k_{dis} E_{dis}^{\prime} + k_{rep} E_{rep}^{\prime}$$

Where,  $E_{ele}$  represents the electrostatic energy,  $E_{pol}$  is the polarization energy,  $E_{dis}$  is the dispersion energy and  $E_{rep}$  is the repulsive energy. k's in the above equation are the scale factors corresponding to the molecular energies obtained from the generated wave function using density functional theory. Further, the interaction energies were employed to construct '3D-energy frameworks', which can be used to visualize the packing of the molecules in the molecular crystal structures [26–29].

# 2.5. Quantum theory of atoms in molecule (QTAIM) analysis

The QTAIM analysis is a computational method used to study

intramolecular interactions by examining the electron density topology in interatomic regions [30]. The analysis is based on two scalar fields: electron density ( $\rho(r)$ ) and reduced density gradient (RDG). These fields are used to map the bonding properties within the molecule. Specifically, QTAIM analysis focuses on several properties at the bond critical point (BCP), including electron density ( $\rho(r)$ ). We utilize *Multiwfn* and *VMD* computational software to perform this analysis [31–34].

# 2.6. Density functional theory (DFT) calculations

DFT calculations are a crucial tool in understanding the molecular mechanisms and behaviour of compounds. Here, we used a widely used electronic structure modelling software, *Gaussian 16* [35] to perform quantum chemical calculations to predict various molecular properties. The calculations were carried out using Becke's three-parameter hybrid functional and Lee–Yang–Parr correlation hybrid functionals B3LYP along with 6-311+G (d,p) a double-ζ Pople type basis set for non-metal atom and LANL2DZ (Los Alamos National Laboratory 2 Double-Zeta) for metal, basis set was used for geometrical optimization [36,37] to investigate the molecular system of the title compound via geometry optimization and frequency calculations [36]. The HOMO-LUMO energy gap and MEP were generated and visualized using the *Gauss view* software [38–40].

## 2.7. Molecular docking

The crystal structure serves as the primary input for conducting molecular docking studies to explore residue interactions, including hydrogen bonds and other interactions, in conjunction with binding energy scores. The initial configuration of the PDB 3D structure (1JIL: Crystal structure of *S. aureus TyrRS*) was acquired from the Protein Data Bank (www.rcsb.org) [41]. Preprocessing of the protein involved removing existing ligands and adding polar hydrogens, followed by the application of Kollman's united atomic charges using *Autodock Vina* [42]. Subsequently, the protein and ligand were saved in a .pdbqt format file. Conformational poses of the copper complex were generated by utilizing the orientations within the active site of 1JIL through the Lamarckian genetic algorithm. The identification of optimal poses relied on binding affinity, and pose retrieval was facilitated using the non-bonding interaction visualizer in *Discovery Studio* [43].

# 2.8. Antibacterial activity

The disc diffusion method is a common technique for evaluating antimicrobial activity. Mueller-Hinton agar is poured onto glass petri plates and left to solidify. A standardized inoculum of the test organism is evenly spread on the plates using a sterile cotton swab. Four discs, each 5 mm in diameter and spaced 20 mm apart, are then placed on the plate. These discs contain the antibiotic, negative control, and two test samples (T1 and T2). The plates are incubated for 24 h at 36  $^{\circ}\text{C} \pm 1~^{\circ}\text{C}$  under aerobic conditions. Following incubation, the zone of bacterial growth inhibition around the discs is measured in millimetres.

To prepare discs T1 and T2, the samples are diluted to create a stock solution of 10 mg/ml. A measured quantity of the samples (50 and  $100\mu L$ ) from the stock solution is then transferred to sterile filter paper discs and allowed to dry at room temperature. The variation in the different parameter were taken into the account by refering EUCAST guidelines [44,45].

For the culture media, Mueller Hinton Agar medium (HIMEDIA-M173) is utilized. This is prepared by suspending 38 g in 1000 ml of distilled water, boiling until fully dissolved, sterilizing via autoclaving at 15 lbs pressure (121  $^{\circ}\text{C}$ ) for 15 min, cooling to 45–50  $^{\circ}\text{C}$ , and subsequently pouring into sterile petri plates [27,46].

#### 3. Results and discussions

## 3.1. Synthesis and characterization

A methanolic solution of the Schiff base ligand was combined with a methanolic solution of copper acetate monohydrate. The resulting red reaction mixture was refluxed, leading to the formation of a dark red precipitate, which was subsequently filtered. Crystals of the copper complex were then obtained through slow evaporation of the solvent. The formation of the copper complex confirmed by vibrational analysis and elemental analysis. SEM imaging revealed that the copper complex exhibits a rectangular morphology.

## 3.2. Single crystal X-ray ray diffraction

The crystal structure analysis of the metal complex has revealed that the copper complex with molecular formula  $[\text{Cu}(\text{C}_{14}\text{H}_{11}\text{BrNOS})_2]$  crystallized as a bidentate ligand complex in the monoclinic crystal system with a centrosymmetric space group  $P2_1/c$ . The azomethine carbonyl chain (N1=C7 of bond length 1.273 Å) of the ligand connects the thioanisole and 4-bromophenol ring. The dihedral angle of  $68.36^{\circ}$  between thioanisole and 4-bromophenol molecules shows nonplanarity of the ligand present in the complex and it was observed that this is due to the steric effect of the methyl sulfide and bromo group present on the opposite side of the ligand (Figure S3). The ORTEP of the metal complex is shown in Fig. 1, and the crystallographic data and structure refinement statistics are given in Table 1.

In a four-coordinated complex, the two largest angles,  $\alpha$  and  $\beta$ , are used to determine the geometry index  $(\tau_4)$  value of the complex [47]. The Cu(II) complex has a perfect square planar geometry, which is evident by the  $\tau_4$  value of 0. By comparing the  $\tau_4$  values reported in previous literature, we observe that the likelihood of achieving a perfect square planar geometry is higher in molecules with inversion symmetry, which is also true for our molecules (Molecules 4, 6, and 7 in Table S1). Additionally, functional groups near the chelating ring create steric hindrance, leading to distortions in the square planar geometry (Molecule 10 in Table S1). The torsion angle made by the atoms

**Table 1**Crystal structure and refinement parameters of the copper complex.

Parameter	Copper Complex
Empirical formula	[Cu (C <sub>14</sub> H <sub>11</sub> BrNOS) <sub>2</sub> ]
Formula weight	352.98
Temperature (K)	293(2)
Wavelength (Å)	$\lambda = 0.71073$
Crystal system, space group	Monoclinic, $P2_1/c$
Unit cell dimensions	
<i>a</i> (Å)	10.429(9)
<i>b</i> (Å)	11.230(9)
c(Å)	11.885(10)
$lpha(^{\circ})$	90.000(10)
$\beta(^{\circ})$	104.220(17)
$\gamma(^{\circ})$	90.000(17)
Volume (Å <sup>3</sup> )	1349(2)
Density (g cm <sup>-3</sup> )	1.738
Absorption coefficient (mm <sup>-1</sup> )	3.955
$F_{000}$	702.0
Crystal size (mm <sup>3</sup> )	$0.37\times0.31\times0.26$
$2\theta$ range for data collection (°)	6.994 to 49.984
Index ranges	$-6 \le h \le 12$
	$-13 \le k \le 13$
	$-14 \le l \le 13$
Reflections collected	5608
Independent reflections	2354
Data/restraints/parameters	2354/0/170
Goodness-of-fit on F <sup>2</sup>	1.019
Final $[I > 2\sigma(I)]$	$R_1 = 0.0808, wR_2 = 0.1862$
R indices (all data)	$R_1 = 0.1579, wR_2 = 0.2284$
Largest diff. peak and hole (e Å <sup>-3</sup> )	0.77/-0.98
CCDC deposit No.	2352425

C1-O1-Cu1-N1 is  $-136.6^{\circ}$  indicating *-synclinal* conformation and the torsion angle formed by the atoms C7-N1-Cu1-O1 is  $-151.0^{\circ}$  which is in *-synperiplanar* conformation. The puckering analysis revealed that the chelating ring, Cg1(C1, C6, C7, N1, O1,Cu1) adopts a half chair conformation Figure. S2(a) with puckering parameters Q(2)=0.430(8) Å, Q(3)=-0.216(9)Å and  $\phi(2)=198.6(12)^{\circ}$ . Further, the half-chair conformation of Cg1 intersects with the symmetry generated Cg2 at the Cu atom of the complex, leading to the formation of chair-like

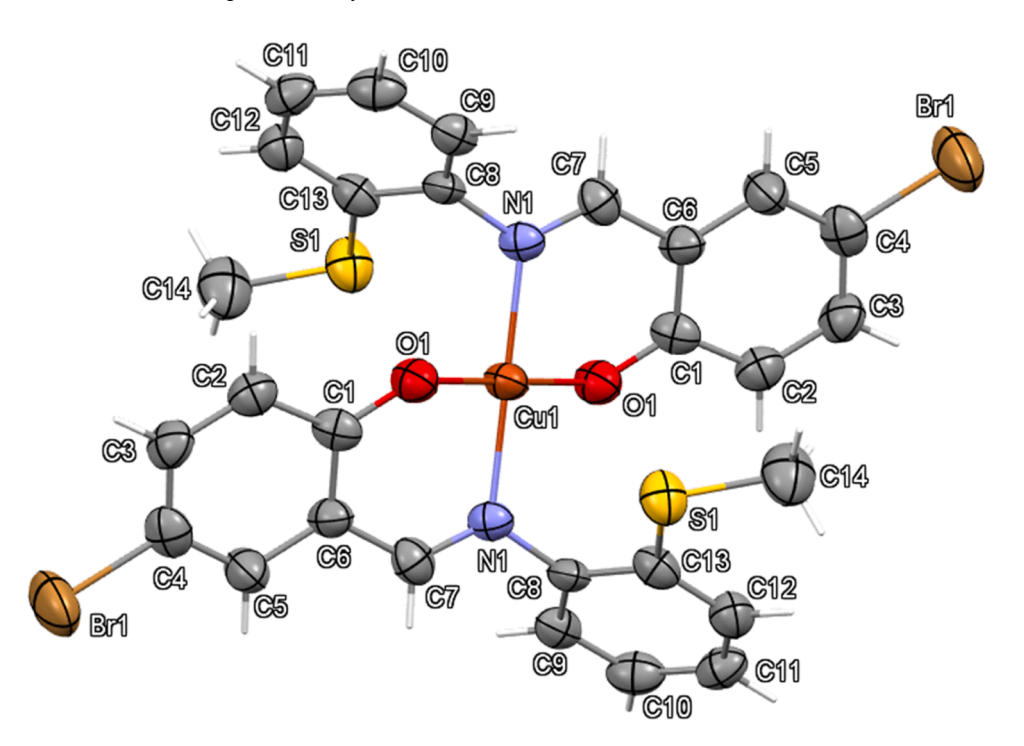


**Fig. 1.** ORTEP diagram of the copper complex with thermal ellipsoids drawn at 50 % probability. The dimeric molecule is generated by the symmetry operation -x, 1-y, -1-z.

conformation [3] Figure S4.

Crystal structure analysis also revealed the contribution of shortest inter-molecular contacts, which is summarized in Table 2. C14-H14···Br1 short interaction interconnects two molecules along the crystallographic *b*-axis, resulting in the formation of a 1-D zigzag chain (Fig. 2). Further, the adjacent chains connect through the same type of contact, leading to the formation of 2-D sheets along the same crystallographic plane. Further, 2-D sheets are interconnected by the C11-H11···C14/H14B interaction to form 3D supramolecular architecture (Fig. 3).

Further, the short ring interaction analysis between the centroid of the ring molecules revealed the presence of three distinct Cg···Cg interactions and one lone pair-Cg interaction (Table S5). Centroids Cg3 (C1–C6) and Cg4 (C8–C13) were found connected through  $\pi$ ··· $\pi$  interaction namely; Cg3···Cg4 (4.453 Å, 42.3° and -x,1/2 + y,1/2-z), Cg3···Cg4 (4.614 Å, 42.3° and x,1/2-y,1/2 + z) and Cg4···Cg3 (5.105 Å, 40.8° and -x,1-y,1-z). This shows the importance of Cg.···Cg interactions in stabilizing the crystal structure of the metal complex (Fig. 4). Furthermore, the single crystal structure analysis also revealed the presence of C9–H9····Cg3 interaction with the distance of 3.490 Å (x,1/2-y,-1/2 + z). The geometrical parameters of the complex, such as bond length, angle and torsion angles, are tabulated in Table S2-S4.

## 3.3. Hirshfeld surface analysis

Hirshfeld surface analysis (HSA) was carried out to investigate the quantitative analysis of the intermolecular interactions in the crystalline environment. HSA is also useful to understand the nature and individual contributions of each intermolecular interaction.

The  $d_{\mathrm{norm}}$  plots were mapped with a colour scale between -0.0757 a. u. (blue) to 1.115 a.u. (red), respectively. The calculated volume inside the Hirshfeld surface is found to be 665.48 ų in the area of 509.36 Ų with globularity (G) 0.724, asphericity ( $\Omega$ ) 0.138. Further,  $d_{\mathrm{i}}$  (1.0514 au to 2.6992 a.u.),  $d_{\mathrm{e}}$  (1.0534 to 2.6884 a.u.), shape index (-1.0 a.u. to +1.0 a.u.), curvedness (-4.0 a.u. to +0.4 a.u.) and fragment patch (0.0 a.u to 13.00 a.u) surface mapped on the Hirshfeld surface of the molecule are as shown in Fig. 5.

The  $d_{norm}$  HS of the copper complex consists of a pair of identical dark red circular spots shown by green and yellow circles in Fig. 5(a) highlighting the C14-H14···Br1 contacts. In addition, we also observed other intermolecular interactions which are highlighted in red colour, which are in good agreement with the experimental result.

The pattern of red and blue triangles on the shape index surface, highlighted by black coloured circles (Fig. 5), shows the presence of characteristics of Cg(3)···Cg(4) stacking interactions between the centroids of the aromatic rings in the crystal structure of the complex. The blue triangles represent convex regions resulting from the presence of ring carbon atoms of the molecule inside the surface, while the red triangles represent concave regions caused by carbon atoms of the  $\pi$  –stacked molecule above it.

The root mean square value of the curvature for the surface is the curvedness (low with flat area and high with sharp curvature), which divides the surface into contact patches with the nearest molecule and are shown as relatively large green planes on the curvedness surface. These flat regions on the surface over the ring structures (highlighted by arrows) present in the Cu-complex indicate the  $\pi \cdots \pi$  stacking interactions. The fragment patches provide a suitable method for

**Table 2**Summary of shortest interconnects in copper complex crystal structure.

Type	D-H···A	D-H	H…A	D···A	D-H···A
Inter	C14–H14B···Br1 <sup>i</sup>	0.960	2.965	3.806(1)	147.00
Inter	C11-H11···C14 <sup>ii</sup>	0.936	2.819	3.699 (8)	158.36
Inter	C14-H14B···C11 <sup>ii</sup>	0.96	2.762	3.699(8)	83.50

 $<sup>-</sup>x,-1/2+y,-1/2-z^{i}-1-x,1/2+y,-3/2-z^{ii}$ .

discerning the nearest neighbouring coordination. The identification of the nearest neighbouring coordination environment of the molecules is facilitated by observing the colour patches on the Hirshfeld surface, indicating their proximity to adjacent molecules (Fig. 5).

The expanded 2D fingerprint plots (FPs) of the metal complex were drawn in the range of 0.9 –2.6 Å view with the  $d_e$  and  $d_i$  distance scales displayed on the graph axes. The analysis of 2D-FPs reveals the quantitative contributions of molecular contacts to the total Hirshfeld surface. From the analysis, it was found that among all possible contacts between the atoms, the major contribution to the Hirshfeld surface is from the H···H contacts, which contributed 36.2 % to the total Hirshfeld surface. This was witnessed by the asymmetrically scattered points, which cover a large region of the FP plot with two short and broad peaks at  $d_{\rm e}+d_{\rm i}\approx 1.2$  Å, as shown in Fig. 6. This is due to the presence of an abundance number of hydrogen atoms very close to the molecular surface. The second highest contribution was due to Br...H (21.8 %) contacts, which is represented by a pair of wings with tips at  $d_e + d_i \approx 2.9 \text{ Å}$ and the next equally important contribution is from C···H (20.8 %). It shows the presence and contribution of C—H $\cdots\pi$  type of intermolecular interaction. Various other interconnects in the structure are S.-. H (7.5 %), H...O (6.2 %), Br...C (2.8 %) and C...C (2.7 %) contacts were shown in the form of traces on the 2D-FPs. Further, the significant contribution from C···C interactions, represented as a bullet-shaped pattern, shows the presence and the role of  $\pi \cdots \pi$  stacking interactions in the formation and stabilization crystal structure of the title metal complex molecule. The enrichment ratio (ER) analysis reveals that Br...H and O...H intermolecular contacts are favoured in structure. The  $E_{xv}$  value for the contacts present in the Schiff base complex is listed in Table 3. An Exv value larger than unity indicates a high propensity for this contact to form in the supramolecular packing. Although the percentage contribution of interatomic H···H contacts to HS is higher, the enrichment ratio analysis shows that H···H contacts are less than unity. This discrepancy is due to random contacts being expressed more than actual contacts. Since hydrogen atoms are already enriched with Br...H and O···H interactions, this eventually reduces the prevalence of H···H contacts.

# 3.4. Interaction energies and 3D energy frameworks

The total interaction energy for the Cu complex was calculated by generating the molecular cluster of radii 3.8 Å around the selected molecule. The symmetry operations were employed in the energy framework calculations to compute the molecular wave functions. The total interaction energy for the Cu complex was calculated by energy frameworks analysis and is found to be equal to -96.881 kJ/mol. This total interaction energy of the molecule is the algebraic sum of electrostatic (-30.77 kJ/mol), polarization (-9.43 kJ/mol), dispersion (-98.83 kJ/mol) and repulsive (42.17 kJ/mol) energies. The energy framework calculations revealed that the dispersion energy dominates over the electrostatic and polarization energies in the crystalline environment of the compound (Fig. 7, Table S6).

# 3.5. QTAIM analysis

In recent years, the QTAIM framework has emerged as a robust tool for delving into a more precise and quantitative understanding of intramolecular interactions based on electron density ( $\rho(r)$ ). Within NCI analysis, the  $sign(\lambda 2)$  parameter proves highly useful in discerning the nature of bonding. In the 2D RDG scatter plots (Fig. 8), when  $sign(\lambda 2) < 0$  (blue), it signifies a bonded interaction. A  $sign(\lambda 2)$  value approximating zero (green) and  $sign(\lambda 2) > 0$  (red) denote van der Waals and nonbonding interactions, respectively. Notably, the presence of a greencoloured iso-surface in both 3D and 2D plots suggests the existence of van der Waals interactions between the copper and sulfur atoms, implying the sulfur atom's propensity for coordination bonding. Additionally, the red-colored iso-surface observed within the metalocyclic

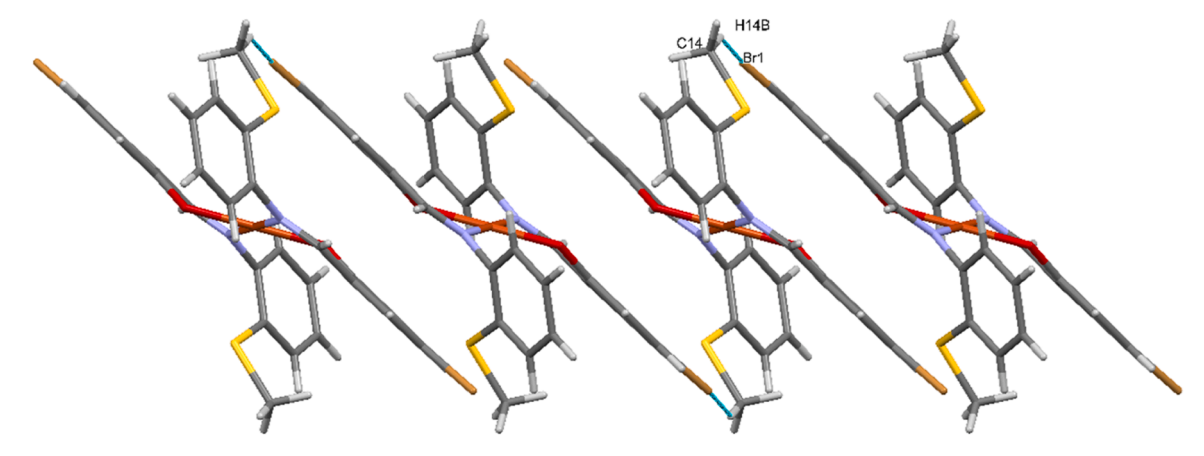
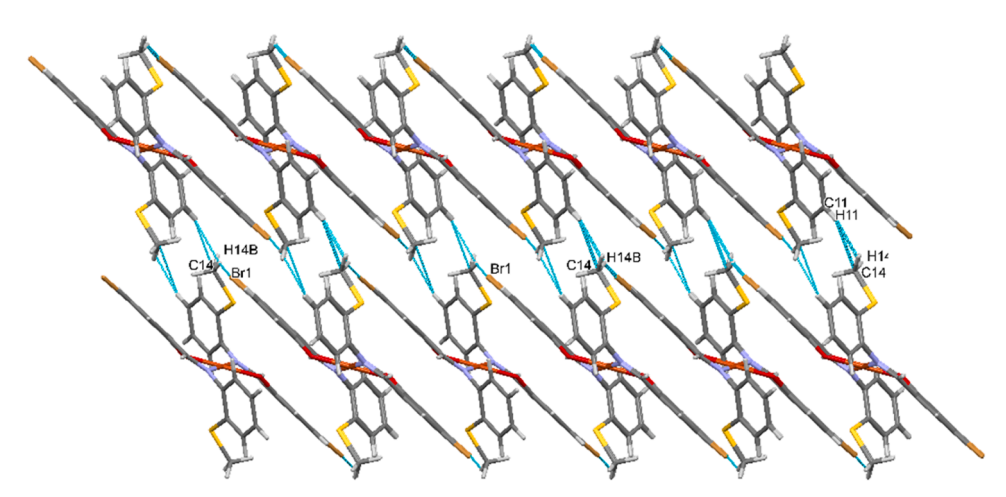


Fig. 2. 1-D molecular packing of the complex.



 $\textbf{Fig. 3.} \ \ \text{3-D supramolecular packing of the complex.}$ 

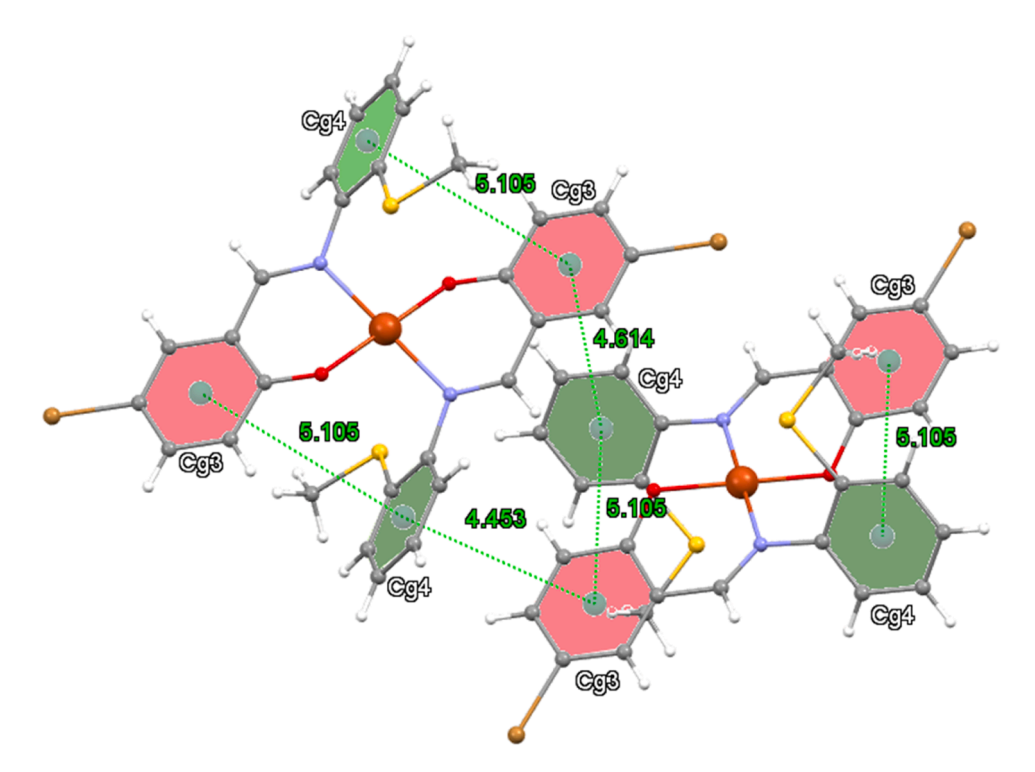
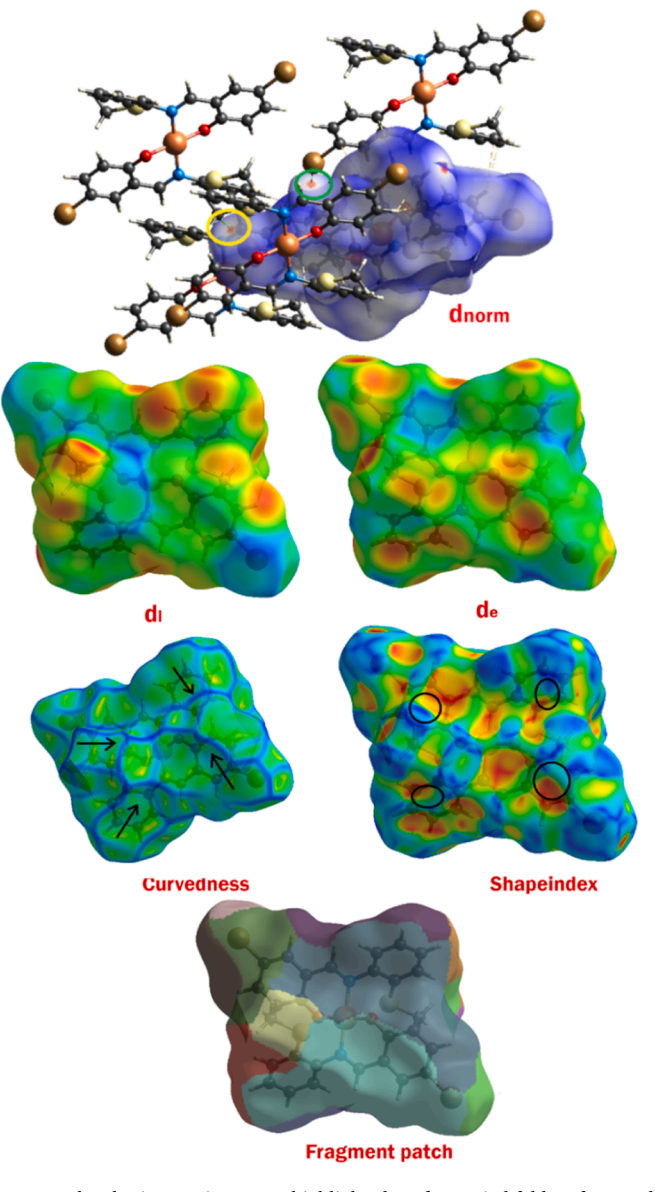


Fig. 4.  $Cg \cdots Cg$  staking interactions present in the complex.



**Fig. 5.** Molecular interactions were highlighted on  $d_{\text{norm}}$  Hirshfeld surface, and the  $d_{\text{i}}$ ,  $d_{\text{e}}$ , curvedness, Shape index, and fragment patch surfaces were mapped on the Hirshfeld surface of the molecule.

ring indicates a pronounced steric effect, indicative of the presence of a strong chelating ring.

# 3.6. DFT studies

The optimization was performed in the doublet state, and the structural conformation was compared with the crystal structure. A good correlation was observed between the calculated bond lengths, bond angles, and torsional angles and the experimental data, indicating the accuracy of the computational model.

Additionally, molecular properties of the compound were explored using the concept of molecular orbitals (MOs), which are fundamental in understanding a molecule's stability and reactivity. In the complex, the HOMO is predominantly located around the bromo-substituted phenyl ring and chelating rings of the ligand in both  $\alpha$  and  $\beta$  MOs. The energy levels of the HOMO are approximately -5.6670 eV for  $\alpha$  and -5.6200 eV for  $\beta$  (Fig. 9). On the other hand, the LUMO is spread over the entire molecule in the  $\alpha$  MO, with an energy value of -2.0074 eV, while in the  $\beta$  MO, it is localized on the metal atom and chelating ring atoms, with an

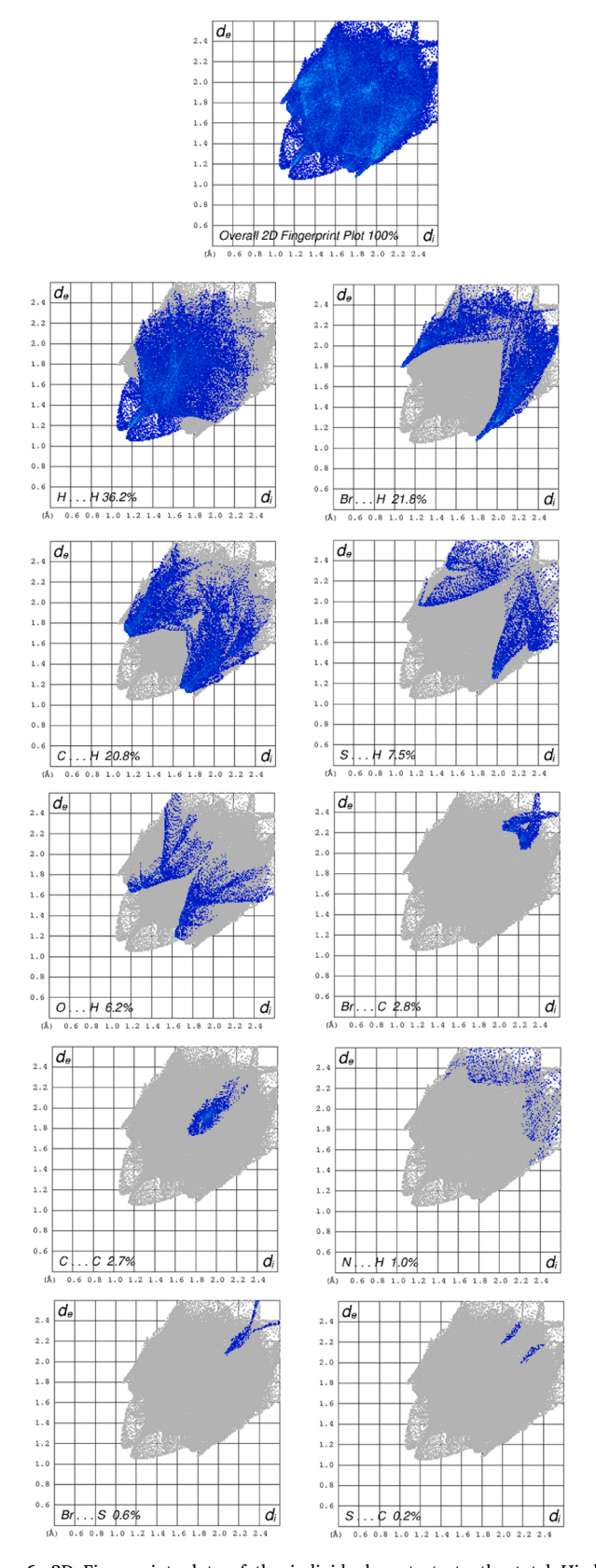


Fig. 6. 2D Fingerprint plots of the individual contacts to the total Hirshfeld surface.

**Table 3**The percentage contribution of individual interaction and enrichment ratio.

	Н	C	Br	О	N	S	Cu
Н	31.6						
C	8.8	6.8					
Br	22.3	1.6	0.6				
O	18.3	0.6	1.5	0			
N	0.6	1.4	0	0	0		
S	2.3	1.9	0.4	0	0	0	
Cu	0.5	0.8	0	0	0	0	0
	84.4	13.1	2.5	0	0	0	0
CXY	52.8	15.1	25.8	20.4	2	4.6	1.3
Sx	58	14.35	13.5	10.2	1	2.3	0.65
H	33.64						
C	16.65	2.06					
Br	15.66	3.87	1.82				
O	11.83	2.93	2.75	1.04			
N	1.16	0.29	0.27	0.20	0.01		
S	2.67	0.66	0.62	0.47	0.05	0.05	
Cu	0.75	0.19	0.18	0.47	0.05	0.03	0.01
EXX							
H	0.9						
C	0.5	3.3					
Br	1.4	0.4	0.3				
O	1.5	0.2	0.5	0.0			
N	0.5	4.9	0.0	0.0	0.0		
S	0.9	2.9	0.0	0.0	0.0	0.0	
Cu	0.7	4.3	0.0	0.0	0.0	0.0	0.0

energy value of -3.0474 eV. A significant energy difference of 2.5726 eV was observed between the HOMO and LUMO of the  $\beta$ -spin. This energy difference provides valuable information about the stability and electronic properties of the molecule, particularly regarding its reactivity and potential for electronic transitions (Table 4) [48]. Further, The HOMO-LUMO energy gap (Eg) is an established parameter for measuring the extent of intramolecular charge transfer and has been used in pharmaceutical studies. In this study, the compounds exhibited antimicrobial activity, which may be attributed to lower LUMO energy level (2.0074 eV) [49,50] .

The MEP map visually represents the electrostatic potential on the molecular surface, which is crucial for identifying regions with high and low electrostatic potential. The chelating oxygen atoms, sulfur atom, and the substituted bromine atom in the ligand exhibit high electronegative potential, with values of -0.0393 a.u., -0.0212 a.u., and -0.0162 a.u., respectively. These regions are considered electrophilic, indicating that they are likely to attract electrons from the surroundings. On the other hand, regions with low electrostatic potential are typically nucleophilic in nature. Specifically, the -CH group of the chelating ring and substituted phenyl ring exhibit positive electrostatic potential values of +0.0270 a.u. and +0.0187 a.u., respectively (Fig. 10). Additionally, the -CH3 group of the alkyl sulfide moiety has a positive electrostatic potential value of +0.0221 a.u. These regions are more likely to donate electrons during chemical reactions. The electrostatic potential values of the active sites in the studied compounds can be utilized in docking studies. These values play a significant role in generating docking poses within the binding pockets of proteins. Therefore, the results obtained from molecular electrostatic potential (MEP) analysis can be valuable for assessing the biological activity of the compounds [50].

#### 3.7. Antibacterial activity

The explore antimicrobial efficacy against <code>Staphylococcus</code> <code>aureus</code>, we employed a disc diffusion assay, a commonly utilized method for evaluating compound activity. At a concentration of 500  $\mu g$ , the Schiff base compound exhibited a zone of inhibition measuring 9 mm. Remarkably, this zone expanded to 14 mm at a higher concentration of 1000  $\mu g$  (Figure S5). Compered with standard Gentamycin (160  $\mu g/25$  mm) our compound shows moderate zone of inhibition. Further, similar

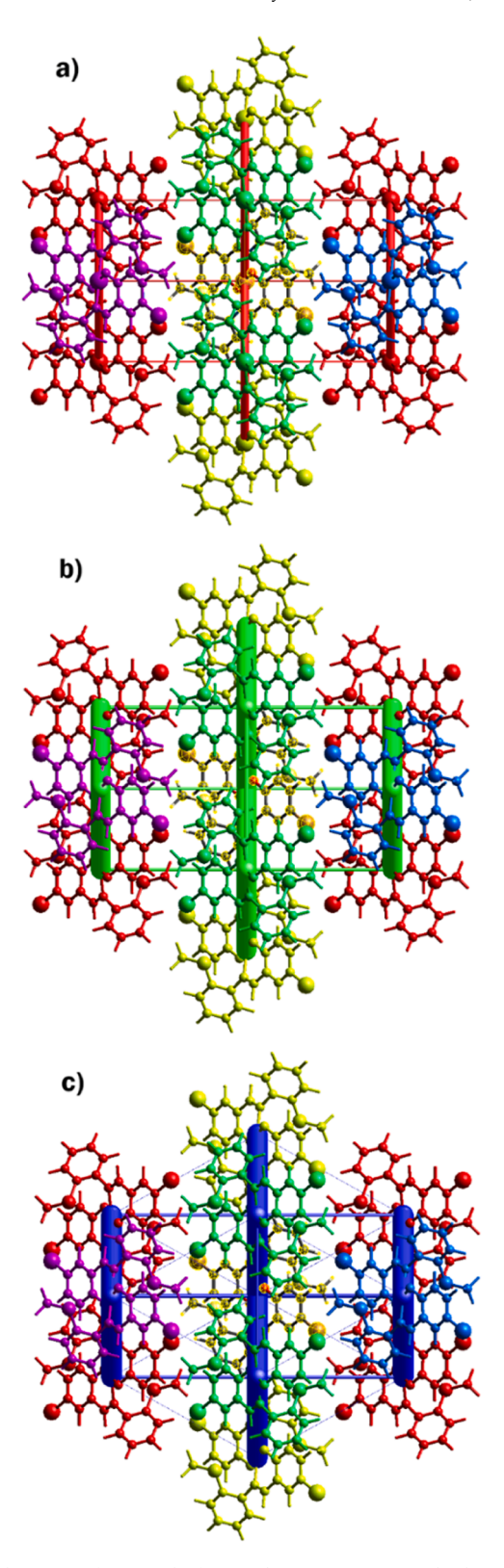


**Fig. 7.** The energy frameworks for (a) electrostatic energy, (b) dispersion energy and (c) total energy of the molecule.

compounds were also reported againts *Staphylococcus aureus* which also supports the above reuslts. These findings underscore the substantial antimicrobial effectiveness of the Schiff-base derivative against *S. aureus* bacteria [51,52]. The increased antibacterial activity of the copper complex can be explained by Tweedy's chelation theory. According to

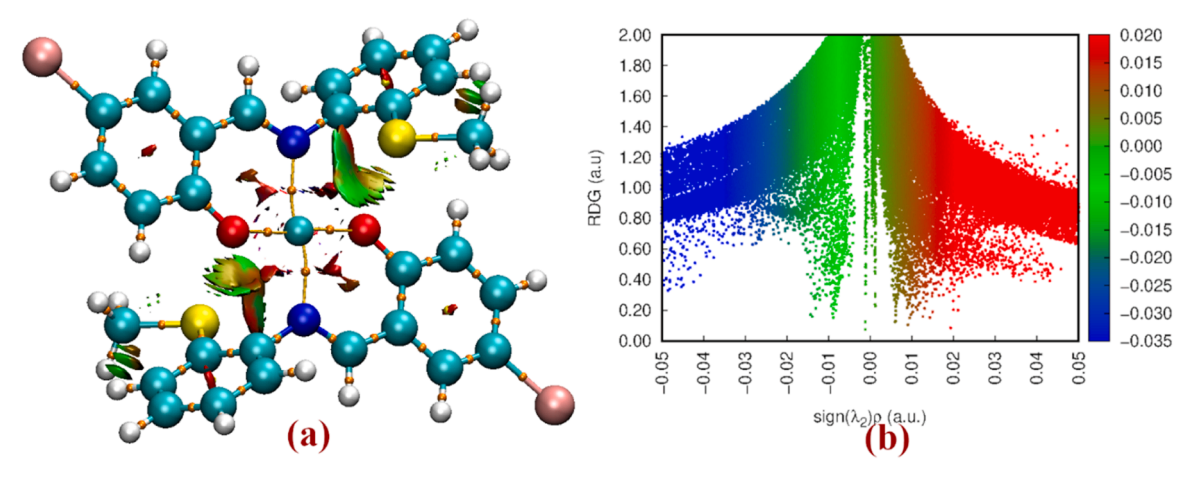


Fig. 8. The (a) 3D and (b) 2D QTAIM+NCI plot of copper complex.

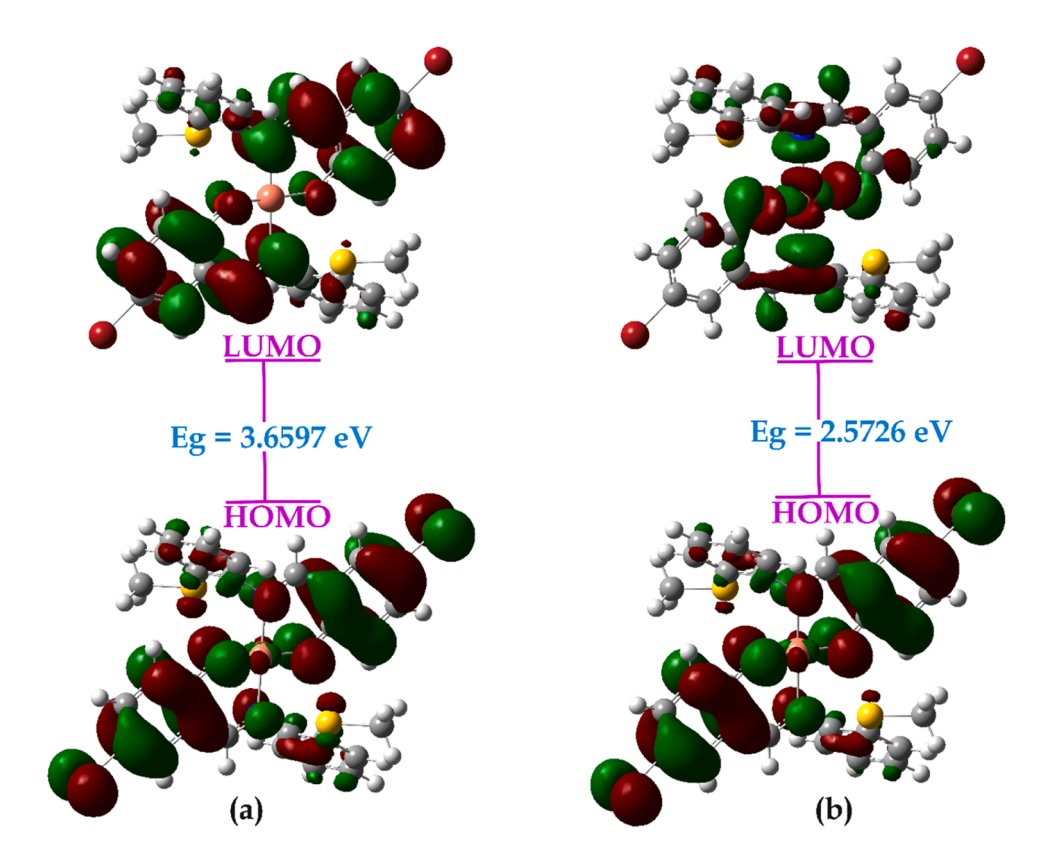


Fig. 9. Frontier molecular orbitals along with energy gap of (a) alpha spin and (b) beta spin.

**Table 4**The chemical reactive parameter of the complex.

Name	alpha	beta
E <sub>homo</sub> (Hartree)	-0.2082	-0.2065
E <sub>lumo</sub> (Hartree)	-0.0737	-0.1119
E <sub>homo</sub> (eV)	-5.6670	-5.6200
E <sub>lumo</sub> (eV)	-2.0074	-3.0474
Energy gap (Eg)	3.6597	2.5726
Ionization energy (I)	5.6670	5.6200
Electron Affinity (A)	2.0074	3.0474
Electronegativity (χ)	3.8372	4.3337
Chemical Potential (µ)	-3.8372	-4.3337
Global hardness (η)	1.8298	1.2863
Global softness (s)	0.5465	0.7774
Electrophilicity index(ω)	4.0234	7.3004

this theory, the reduced polarity on the copper chelating ring arises from the sharing of the partial positive charge on the copper metal with donor groups (N and O), along with the significant delocalization of  $\pi\text{-electrons}$  on the chelate ring. This redistribution of polarity enhances the lyophilic character of the copper complex, allowing it to penetrate the lipid membrane. This penetration disrupts the permeability barrier of the bacterial cell wall, interfering with normal cellular processes and respiration in microorganisms, ultimately causing cell lysis and inhibiting bacterial growth [53,54].

# 3.8. Molecular docking studies

The antibacterial activity of copper complex against of *S. aureus TyrRS* is evaluated by molecular docking studies. To tackle bacterial infection problems, novel therapeutic agents need to be designed and

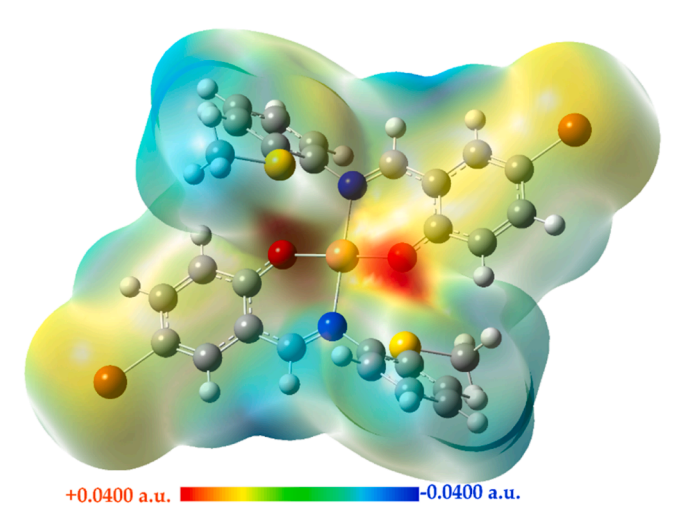


Fig. 10. Molecular electrostatic potential map of the copper complex.

this can be achieved with the aid of ligand-protein in-silico studies. The amino acid sequences of S. aureus TyrRS has helix H5 and strand D. S. aureus TyrRS contains three domains: the N-terminal  $\alpha/\beta$  domain, the  $\alpha$ -helical domain, and a disordered C-terminal domain, connected by a linker peptide. S. aureus TyrRS has two residues at the N-terminus that are distant from the active site and likely non-functional [41]. The copper complex is docked to the active site of the S. aureus TyrRS. A good binding score of -7.6 kcal/mol was observed, and corresponding protein-ligand interactions were observed in the Fig. 11(b), (c). The protein binds to the sulphur atom of the copper complex with a conventional hydrogen bond through THR169 (2.98 Å) (Fig. 11). The bromine atom also interact with two amino acids such as MET 77 and TYR 165. The other interactions, such as  $\pi \cdots \pi$ , alkyl and  $\pi$ -alkyl are depicted in the Fig. 11(c).

## 4. Conclusion

Bi-dentate novel Cu(II) complex were synthesized and characterized by spectroscopic techniques. X-ray diffraction analysis reveals the perfect square planar geometry around Cu(II) ion. The higher nonplanarity of a copper complex is confirmed by the dihedral angle of 40.84°. Puckering analysis of copper chelating ring is in the half-chair conformation. The Cu(II) complex has a perfect square planar geometry with the value of  $\tau_4$  =0. The multi-dimensional supramolecular assemblies are formed by H···H, C—Cl··· $\pi$  and C—H··· $\pi$  interactions and it is also supported by Hirshfeld surface analysis. NCI analysis shows the coordination bond between Cu—O is stronger compared to Cu—N. NBO analysis reveals the charge transfer between the ligand-metal and exhibits partial covalent bond character. The metal chelates are more effective antimicrobial agents than their parent ligands against Staphylococcus aureus and methicillin-resistant Staphylococcus aureus. The docking studies show a strong binding affinity toward the PBP2 protein and support the experiment results.

Appendix A. Supplementary data;

CCDC 2352425 contains the supplementary crystallographic data of the Schiff base compound. The data can be obtained free of cost via <a href="http://www.ccdc.cam.ac.uk/conts/retrieving.html">http://www.ccdc.cam.ac.uk/conts/retrieving.html</a>, or from the Cambridge Crystallographic Data Centre, 12 Union Road, Cambridge CB2 1EZ, UK; fax: (+44) 1223-336-033; or e-mail: deposit@ccdc.cam.ac.uk.

## CRediT authorship contribution statement

Udaya Kumar AH: Writing – review & editing, Writing – original draft, Visualization, Validation, Software, Investigation, Data curation, Conceptualization. Mahesha: Writing – review & editing, Writing – original draft, Visualization, Validation, Software, Investigation, Data curation, Conceptualization. Jyothi KL: Writing – original draft, Visualization, Software. Akil Ahmad: Funding acquisition, Methodology, Resources. Mohammed B Alshammari: Conceptualization, Funding acquisition, Resources. Karthik Kumara: Conceptualization, Formal analysis, Software, Writing – original draft. Lokanath NK: Writing – review & editing, Supervision, Investigation, Conceptualization.

## Declaration of competing interest

The authors declare that they have no known competing financial interests or personal relationships that could have appeared to influence the work reported in this paper.

## Data availability

The authors are unable or have chosen not to specify which data has

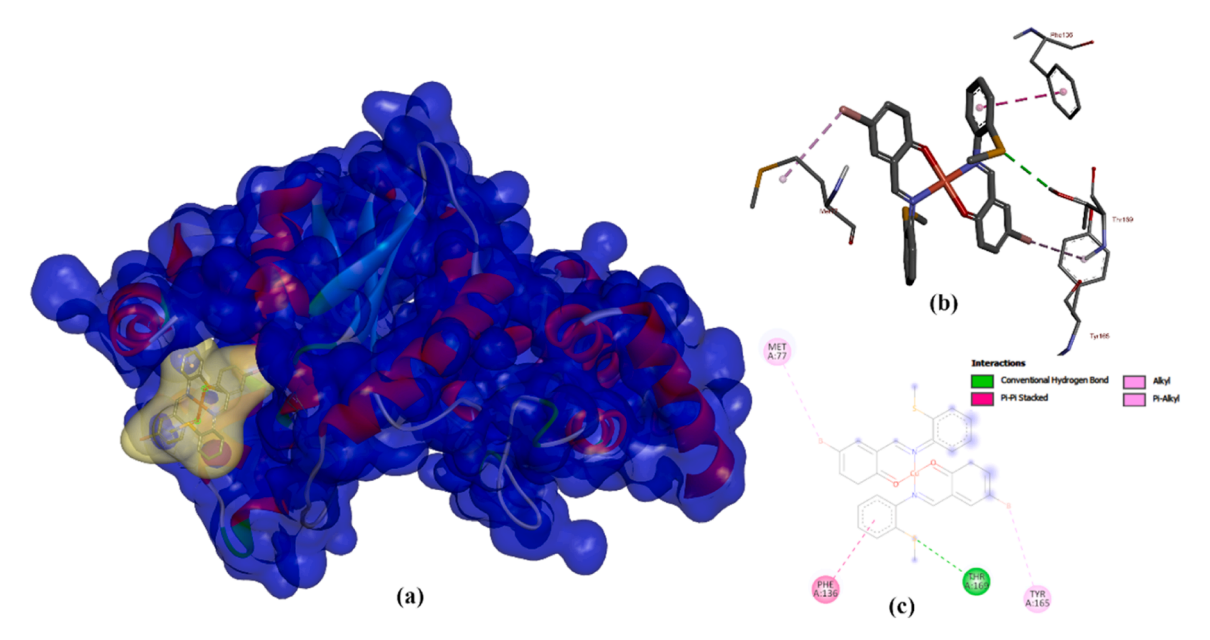


Fig. 11. (a)The complex binding the protein pocket and (b, c) 3D-2D protein-ligand interactions.

#### been used.

CCDC No. 2352425 (Original data) (CCDC)

## Acknowledgements

The authors are thankful to the DST-FIST program (*SR/FST/PSI-119/2019*), National Single Crystal Diffractometer Facility, DoS in Physics, CPEPA, and DST-PURSE, Vijnana Bhavan, University of Mysore, Mysuru. This study is also supported via funding from Prince sattam bin Abdulaziz University project number (PSAU/2024/R/1445)

#### Supplementary materials

Supplementary material associated with this article can be found, in the online version, at doi:10.1016/j.molstruc.2024.139264.

#### References

- P.G. Cozzi, Metal-Salen Schiff base complexes in catalysis: practical aspects, Chem. Soc. Rev. 33 (2004) 410–421. https://doi.org/10.1039/B307853C.
- [2] T.R. Cook, P.J. Stang, Recent developments in the preparation and chemistry of metallacycles and metallacages via coordination, Chem. Rev. 115 (2015) 7001–7045, https://doi.org/10.1021/CR5005666.
- [3] A.H. Udaya Kumar, K. Kumara, N.V. Harohally, K.J. Pampa, N.K. Lokanath, Square planar trans-N2O2 Cu(II) complex: synthesis, crystal structure, Hirshfeld surface, DFT, antimicrobial and docking studies, ChemistrySelect 6 (2021) 6240–6255, https://doi.org/10.1002/SLCT.202101149.
- [4] Mahesha, A.H. Udaya Kumar, K.J. Pampa, N.K. Lokanath, The investigation of modification in structural flexibility and coordination modes in a solvent free β-diketone Cu(II) complex by crystal structure and DFT studies, Polyhedron 232 (2023) 116293. https://doi.org/10.1016/J.POLY.2023.116293.
- (2023) 116293, https://doi.org/10.1016/J.POLY.2023.116293.
   [5] C.M. Da Silva, D.L. Da Silva, V. Modolo, R.B. Alves, M.A. De Resende, C.V.B. Martins, A. Ngelo De Fatimafatima, Schiff bases: a short review of their antimicrobial activities, (2010). https://doi.org/10.1016/j.jare.2010.05.004.
- [6] A. Arunadevi, N. Raman, Biological response of Schiff base metal complexes incorporating amino acids—a short review, J. Coord. Chem. 73 (2020) 2095–2116, https://doi.org/10.1080/00958972.2020.1824293.
- [7] R. Antony, T. Arun, S.T.D. Manickam, A review on applications of chitosan-based Schiff bases, Int. J. Biol. Macromol. 129 (2019) 615–633, https://doi.org/10.1016/ LUBIOMAC 2019 02 047
- [8] S. Shekhar, A.M. Khan, S. Sharma, B. Sharma, A. Sarkar, Schiff base metallodrugs in antimicrobial and anticancer chemotherapy applications: a comprehensive review, Emergent. Mater. 5 (2022) 279–293, https://doi.org/10.1007/S42247-021-00234-1
- [9] Z. Hricovíniová, M. Hricovíni, K. Kozics, New series of quinazolinone derived Schiff's bases: synthesis, spectroscopic properties and evaluation of their antioxidant and cytotoxic activity, Chem. Pap. 72 (4) (2017) 1041–1053, https://doi.org/10.1007/S11696-017-0345-Y, 201772.
- [10] H. Muhammad Junaid, M. Batool, F. Wahida Harun, M. Saleem Akhter, N. Shabbir, Naked eye chemosensing of anions by Schiff bases, Crit. Rev. Anal. Chem. 52 (2022) 463–480, https://doi.org/10.1080/10408347.2020.1806703.
- [11] J. Zhang, L. Xu, W.Y. Wong, Energy materials based on metal Schiff base complexes, Coord. Chem. Rev. 355 (2018) 180–198, https://doi.org/10.1016/J. CCR 2017 08 007
- [12] U. Ndagi, N. Mhlongo, M.E. Soliman, Metal complexes in cancer therapy an update from drug design perspective, Drug Des. Devel. Ther. 11 (2017) 599–616, https://doi.org/10.2147/DDDT.S119488.
- [13] M.A. Said, D.J.O. Khan, F.F. Al-Blewi, N.S. Al-Kaff, A.A. Ali, N. Rezki, M.R. Aouad, M. Hagar, New 1,2,3-triazole scaffold Schiff bases as potential anti-COVID-19: design, synthesis, DFT-molecular docking, and cytotoxicity aspects, Vaccines 9 (2021), https://doi.org/10.3390/VACCINES9091012.
- [14] B. Karska-Wysocki, M. Bazo, W. Smoragiewicz, Antibacterial activity of Lactobacillus acidophilus and Lactobacillus casei against methicillin-resistant Staphylococcus aureus (MRSA), Microbiol. Res. 165 (2010) 674–686, https://do. org/10.1016/J.MICRES.2009.11.008.
- [15] M.K. Hema, C.S. Karthik, Mahesha, K.J. Pampa, P. Mallu, N.K. Lokanath, 4,4,4-trifluoro-1-phenylbutane-1,3-dione metal [Cu(II) and Ni(II)] complexes as an superlative antibacterial agent against MRSA: synthesis, structural quantum-chemical and molecular docking studies, J. Mol. Struct. 1243 (2021) 130774, https://doi.org/10.1016/J.MOLSTRUC.2021.130774.
- [16] H.M. Mahesha, C.S. Krishnegowda, P.J. Karthik, P. Kudigana, L.K. Mallu, Neratur, μ-phenoxide bridged mixed ligand Cu(II) complex: synthesis, 3D supramolecular architecture, DFT, energy frameworks and antimicrobial studies, Polyhedron 185 (2020) 114571, https://doi.org/10.1016/J.POLY.2020.114571.
- [17] CrystalClear: Rigaku Corporation, "CrystalClear Software User's Guide, Molecular Structure Corporation," Rigaku Corporation, 1999, pp. 1718-1725.
- [18] G.M. Sheldrick, Crystal structure refinement with SHELXL, Urn:Issn:2053-2296 71 (2015) 3–8. https://doi.org/10.1107/S2053229614024218.

- [19] G.M. Sheldrick, IUCr, SHELXT integrated space-group and crystal-structure determination, Urn:Issn:2053-2733 71 (2015) 3–8. https://doi.org/10.1107/S20 53273314026370
- [20] A.L. Spek, IUCr, single-crystal structure validation with the program PLATON, Urn: Issn:0021-8898 36 (2003) 7–13. https://doi.org/10.1107/S0021889802022112.
- [21] C.F. MacRae, I. Sovago, S.J. Cottrell, P.T.A. Galek, P. McCabe, E. Pidcock, M. Platings, G.P. Shields, J.S. Stevens, M. Towler, P.A. Wood, Mercury 4.0: from visualization to analysis, design and prediction, J. Appl. Crystallogr. 53 (2020) 226–235, https://doi.org/10.1107/S1600576719014092/GJ5232FIG13THM.GIF.
- [22] P.R. Spackman, M.J. Turner, J.J. McKinnon, S.K. Wolff, D.J. Grimwood, D. Jayatilaka, M.A. Spackman, CrystalExplorer: a program for Hirshfeld surface analysis, visualization and quantitative analysis of molecular crystals, J. Appl. Crystallogr. 54 (2021) 1006–1011, https://doi.org/10.1107/ S1600576721002910.
- [23] Mahesha, M.K. Hema, C.S. Karthik, K.J. Pampa, P. Mallu, N.K. Lokanath, Solvent induced mononuclear and dinuclear mixed ligand Cu(II) complex: structural diversity, supramolecular packing polymorphism and molecular docking studies, N. J. Chem. 44 (2020) 18048–18068, https://doi.org/10.1039/D0NJ03567J.
- [24] K.L. Jyothi, M.K. Hema, K. Kumara, Guru Row, N.K. Lokanath, Structural elucidation of 1:4:4 stochiometric form of thymine – gallic acid cocrystal hydrate: Hirshfeld surface analysis, 3D energy framework, DFT calculations, and SARS CoV-2 docking studies, J. Mol. Struct. 1280 (2023) 135072, https://doi.org/10.1016/J. MOLSTRUC.2023.135072.
- [25] D. Bhat, L. Spoorthy, R. Sharanya, M. Siddesh, A.H. Mahesha, Udaya Kumar, N. K. Lokanath, Influence of hydroxyl group in stabilizing the Schiff base crystal structure: crystal structure, computational and molecular docking studies, J. Mol. Struct. 1280 (2023) 135054, https://doi.org/10.1016/J.
  MOL STRUC 2023 135054
- [26] Mahesha, A.H. Udaya Kumar, K.G. Vindya, K.J. Pampa, K.S. Rangappa, N. K. Lokanath, Structure-property relationship in thioxotriaza-spiro derivative: crystal structure and molecular docking analysis against SARS-CoV-2 main protease, J. Mol. Struct. 1250 (2022) 131746, https://doi.org/10.1016/J. MOLSTRUC.2021.131746.
- [27] M. Siddesh, R. Sharanya, L. Spoorthy, D. Bhat, A.H. Udaya Kumar, Mahesha, M. K. Hema, N.K. Lokanath, Investigation of the molecular basis of halogenated Schiff base derivative by combined crystallographic and computational studies, J. Biomol. Struct. Dyn. (2024), https://doi.org/10.1080/07391102.2023.2301512.
- [28] S.K. Seth, D. Sarkar, A.D. Jana, T. Kar, On the possibility of tuning molecular edges to direct supramolecular self-assembly in coumarin derivatives through cooperative weak forces: crystallographic and hirshfeld surface analyses, Cryst. Growth Des. 11 (2011) 4837–4849, https://doi.org/10.1021/CG2006343/SUPPL FILE/CG2006343 SI 005.CIF.
- [29] S.K. Seth, G.C. Maity, T. Kar, Structural elucidation, Hirshfeld surface analysis and quantum mechanical study of para-nitro benzylidene methyl arjunolate, J. Mol. Struct. (2011) 1000, https://doi.org/10.1016/j.molstruc.2011.06.003.
- [30] J.P. Tidey, V.V. Zhurov, C.G. Gianopoulos, T.S. Hermann, A.A. Pinkerton, QTAIM assessment of the intra- and intermolecular bonding in a Bis(nitramidooxadiazolate) energetic ionic salt at 20 K, J. Phys. Chem. A 122 (2018) 9676–9687, https://doi.org/10.1021/ACS.JPCA.8B10065/SUPPL\_FILE/JP8B10065\_SI\_002. PDF
- [31] T. Lu, F. Chen, Multiwfn: a multifunctional wavefunction analyzer, J. Comput. Chem. 33 (2012) 580–592, https://doi.org/10.1002/JCC.22885.
- [32] A.H. Udaya Kumar, K.J. Pampa, N.V. Harohally, D. Das, B.N. Ghosh, N. K. Lokanath, Structural studies of Schiff base ligand and its copper complexes: solvents effect in 1-D polymeric and monomeric copper (II) complexes, computational and sensing studies, Mater. Chem. Phys. 306 (2023) 128031, https://doi.org/10.1016/J.MATCHEMPHYS.2023.128031.
- [33] C.C. Wu, S. Liu, S. Zhang, Z. Yang, Molcontroller: a VMD graphical user interface featuring molecule manipulation, J. Chem. Inf. Model. 60 (2020) 5126–5131, https://doi.org/10.1021/ACS.JCJM.0C00754.
- [34] S.K. Seth, P. Manna, N.J. Singh, M. Mitra, A.D. Jana, A. Das, S.R. Choudhury, T. Kar, S. Mukhopadhyay, K.S. Kim, Molecular architecture using novel types of non-covalent π-interactions involving aromatic neutrals, aromatic cations and π-anions, CrystEngComm 15 (2013) 1285–1288, https://doi.org/10.1039/ C2CE26577J.
- [35] M. Frisch, G. Trucks, H. Schlegel, G. Scuseria, M. Robb, J. Cheeseman, G. Scalmani, V. Barone, G. Petersson, H. Nakatsuji, X. Li, M. Transport, A. Marenich, J. Bloino, B. Janesko, R. Gomperts, B. Mennucci, H. Hratchian, D. Gaussian, Gaussian 16, Révision B.01, Inc Wallingford CT 6 (2016).
- [36] Y. Yang, M.N. Weaver, K.M. Merz, Assessment of the "6-31+Gt; + LANL2DZ" mixed basis set coupled with density functional theory methods and the effective core potential: prediction of heats of formation and ionization potentials for first-row-transition-metal complexes, J. Phys. Chem. A 113 (2009) 9843–9851, https://doi.org/10.1021/JP807643P/SUPPL\_FILE/JP807643P\_SL003.PDF.
- [37] S.A. Shaikh, S.S. Bhat, V.K. Revankar, N.S. Mahesha, N.K. Loknath, V. Kumbar, Co (II), Ni(II), Cu(II) and Zn(II) complexes of 1,8-naphthalimide-based ligand: syntheses, characterizations and evaluation of antibacterial activities, J. Coord. Chem. 76 (2023) 1586–1603, https://doi.org/10.1080/00958972.2023.2265037.
- [38] Dennington, Roy, Keith, Todd A., Millam, John M., GaussView, Version 6, Semichem Inc., Shawnee Mission, KS, 2016.
- [39] K. Kumara, M.G. Prabhudeva, C.B. Vagish, H.K. Vivek, K.M. Lokanatha Rai, N. K. Lokanath, K. Ajay Kumar, Design, synthesis, characterization, and antioxidant activity studies of novel thienyl-pyrazoles, Heliyon 7 (2021) e07592, https://doi.org/10.1016/J.HELIYON.2021.E07592.
- [40] S.K. Seth, A. Bauzá, G. Mahmoudi, V. Stilinović, E. López-Torres, G. Zaragoza, A. D. Keramidas, A. Frontera, On the importance of Pb $\cdots$ X (X = O, N, S, Br) tetrel

- bonding interactions in a series of tetra- and hexa-coordinated Pb(ii) compounds, CrystEngComm 20 (2018) 5033–5044, https://doi.org/10.1039/C8CE00919H.
- [41] X. Qiu, C.A. Janson, W.W. Smith, S.M. Green, P. McDevitt, K. Johanson, P. Carter, M. Hibbs, C. Lewis, A. Chalker, A. Fosberry, J. Lalonde, J. Berge, P. Brown, C.S. V. Houge-Frydrych, R.L. Jarvest, Crystal structure of Staphylococcus aureus tyrosyl-tRNA synthetase in complex with a class of potent and specific inhibitors, Protein Science 10 (10) (2001) 2008–2016, https://doi.org/10.1110/PS.1800.
- [42] O. Trott, A.J. Olson, AutoDock Vina: improving the speed and accuracy of docking with a new scoring function, efficient optimization, and multithreading, J. Comput. Chem. 31 (2010) 455–461, https://doi.org/10.1002/JCC.21334.
- [43] D.S. Visualizer, Discovery studio visualizer. 2, (2005).
- [44] Sigríður Ólafsdóttir., Comparison of Different Assay Methods and Sample Preparation Procedures for the Evaluation of the Antibacterial Activity of Chitosan. https:// skemman.is/handle/1946/3522.
- [45] A. Åkerlund, E. Jonasson, E. Matuschek, L. Serrander, M. Sundqvist, G. Kahlmeter, E. Dzajic, D.S. Hansen, C.N. Agergaard, A. Pätäri-Sampo, R. Manninen, J. O. Grönroos, J.P. Rasigade, W. Salka, P.H. Boyer, E. Lebessi, N. Zapaniotis, E. Petinaki, I. Spiliopoulou, F. Kolonitsiou, K.O. Helgason, J. Brazil, E. Riccobono, G. Lo Cascio, L. Maccacaro, H. Kolstad, T.S. Haukeland, P.L. Kellokumpu, A. F. Mjøen, S. Tofteland, B. Harbak, S.H. Hartzen, S.H. Hänsgen, K.W. Gammelsrud, U. Skolbekken, N. Michalsen, A.L. Brekken, B. Pedersen, B. Guennigsman, A. Lia, A. K. Berg, F. Marco, C. Pitart, P. Egea, J.L. Cortes-Cuevas, J. Machuca, M. Wietzke, M. Dammström, R. Granström, M. Corneliusson, M. Skarstedt, K. Frykfeldt, C. L. Ivarsson, A. Sergejev, S. Hagström, U. Lidén, J. Rydberg, H. Ramström, I. Fröding, E.A. Petropoulos, K. Ininbergs, S. Jalal, S.L. Persson, N. Kamenska, K. Granlund, A.K. Smekal, A. Hill, G. Rådberg, G. Heyman, L. Rodriguez, L. Vennberg, G. Hazirolan, I. Akyar, G.A. Gelmez, A.N.S. Kaygisiz, A. Åkerlund, EUCAST rapid antimicrobial susceptibility testing (RAST) in blood cultures: validation in 55 European laboratories, J. Antimicrob. Chemother. 75 (2020) 3230-3238, https://doi.org/10.1093/JAC/DKAA333.
- [46] M. Krishnan, D. Dey, C.S.-||| B.J. of, undefined 2019, Antibacterial activity of Weissella confusa by disc diffusion method, Bdpsjournal.Org (n.d.). http://www.

- bdpsjournal.org/index.php/bjp/article/download/729/2836 (accessed April 28, 2024).
- [47] L. Yang, D.R. Powell, R.P. Houser, Structural variation in copper(I) complexes with pyridylmethylamide ligands: structural analysis with a new four-coordinate geometry index, τ4, Dalton Trans. (2007) 955–964, https://doi.org/10.1039/ B617136R
- [48] S.K. Seth, S. Banerjee, T. Kar, Crystal structure and DFT calculations of andrographiside, J. Mol. Struct. 965 (2010), https://doi.org/10.1016/j. molstruc.2009.11.036.
- [49] S. Kumar, V. Saini, I.K. Maurya, J. Sindhu, M. Kumari, R. Kataria, V. Kumar, Design, synthesis, DFT, docking studies and ADME prediction of some new coumarinyl linked pyrazolylthiazoles: potential standalone or adjuvant antimicrobial agents, PLoS One 13 (2018), https://doi.org/10.1371/JOURNAL. PONE.0196016.
- [50] S.A. Elsayed, H.M. El-Gharabawy, I.S. Butler, F.M. Atlam, Novel metal complexes of 3-acetylcoumarin-2-hydrazinobenzothiazole Schiff base: design, structural characterizations, DNA binding, DFT calculations, molecular docking and biological studies, Appl. Organomet. Chem. 34 (2020), https://doi.org/10.1002/ AOC.5643.
- [51] K. Mezgebe, E. Mulugeta, Synthesis and pharmacological activities of Schiff bases with some transition metal complexes: a review, Med. Chem. Res. 33 (2024) 439–463, https://doi.org/10.1007/S00044-024-03192-5.
- [52] H. Kargar, A.A. Ardakani, M.N. Tahir, M. Ashfaq, K.S. Munawar, Synthesis, spectral characterization, crystal structure and antibacterial activity of nickel(II), copper(II) and zinc(II) complexes containing ONNO donor Schiff base ligands, J. Mol. Struct. 1233 (2021) 130112, https://doi.org/10.1016/J.MOLSTRUC.2021.130112.
- [53] R. Ramesh, S. Maheswaran, Synthesis, spectra, dioxygen affinity and antifungal activity of Ru(III) Schiff base complexes, J. Inorg. Biochem. 96 (2003) 457–462, https://doi.org/10.1016/S0162-0134(03)00237-X.
- [54] W. Yu, K.M. Hallinen, K.B. Wood, Interplay between antibiotic efficacy and druginduced lysis underlies enhanced biofilm formation at subinhibitory drug concentrations, Antimicrob. Agents Chemother. 62 (2017), https://doi.org/ 10.1128/AAC.01603-17.